Military Technical College
Kobry El-Kobbah,
Cairo, Egypt.

16th International Conference on Applied Mechanics and Mechanical Engineering.

A MODIFIED VIRTUAL ORIGIN MODEL FOR SHAPED CHARGE JET PENETRATION WITH NON-UNIFORM DENSITY DISTRIBUTION

T. Elshenawy*

ABSTRACT

The penetration of a shaped charge jet is studied in this paper where the jet density deficit is considered. The virtual origin model, which assumes a constant jet density, is modified to include the situation when the jet density deficit causes non-uniform jet density distribution. A relation between the relative density ratio and normalised jet velocity is proposed, based on which an analytical solution of the modified virtual origin model is obtained. The validity of the modified virtual origin model is demonstrated by its largely improved predictions in comparison with experimental and numerical results. It shows that the density deficit term reduces the penetration depth by 19.4%, 12.5% and 12.8% for the un-sintered copper-tungsten powder jet, the solid zirconium jet and the solid copper jet, respectively.

KEYWORDS

Oil well perforator, hydrodynamic jet penetration, virtual origin, non-uniform density distribution.

SYMBOLS AND ABBREVIATIONS

OWP	Oil Well perforator
V.O.	Virtual origin
RHT	The Riedel, Hiermaier and Thoma constitutive model
API-RP	American Petroleum Institute Research Procedures
JWL	Johnes Wilkins and Lee Equation of state of explosives

* Egyptian Armed Forces. Email: tamershenawy@yahoo.com.

INTRODUCTION

Hypervelocity jet of a shaped charge has excellent penetration capability into various targets. Due to its penetration capability, shaped charge has been successfully used both in the battle field to defeat armours and in the oil and gas wells to perforate tunnels to connect the wellbore to the reservoir. In these applications, it is necessary to predict the depth of penetration, which is an important parameter for the assessment of shaped charge effects on a target.

Since the shaped charge jet travels at hypervelocity, the impact of the jet on target produces much higher pressure than the strength of the target, and thus, hydrodynamic model [1-2] can be applied to study the jet penetration. These original hydrodynamic models assumed uniform distributions of jet density and jet velocity along the jet length and applied Bernoulli equation at the interface between jet and target for the pressure equilibrium as shown in Fig.1, i.e.

$$\frac{1}{2}\rho_j(V_j - U)^2 = \frac{1}{2}\rho_T U^2, \quad (1)$$

where V_j is the velocity of a continuous jet; U is the velocity of the jet-target interface or penetration velocity; ρ_j and ρ_t are jet density and target density around the jet-target interface, respectively. When the distributions of jet density and velocity are uniform, the consumption of the jet is controlled by

$$V - U = -\frac{dl}{dt} \quad (2)$$

where l is the current length of jet.

The depth of penetration of the jet into target is determined by:

$$U = \frac{dP}{dt} \quad \text{or} \quad P = \int_0^t U dt, \quad (3)$$

where t=0 is the time when the jet starts to hit the target. The maximum depth of penetration is reached when the jet is completely consumed at $t = t_f$, or $l(t_f) = 0$. For a jet with original length of l_0, the maximum depth of penetration is determined by Eqs.(1-3), i.e.

$$P_{max} = l_0\sqrt{\frac{\rho_j}{\rho_t}}. \quad (4)$$

Equation (4) is also applicable to solid rod penetrator.

For a particulated jet, Bernoulli equation cannot be used directly because the internal pressure cannot be supported when the jet is particulated [1]. Since this paper will only consider continuous jet, the interested reader is referred to [2] for the penetration models of particulated jet.

Since the early time of the jet penetration study, it has been realised that the spatial distribution of jet velocity is not uniform [1]. Birkhoff et al. [1] extended the hydrodynamic penetration model [Eq.(4)] to the jet with non-uniform velocity distribution. However, this model introduced several parameters that cannot be

easily determined, and therefore, it has not been widely used. Abrahamson and Goodier [3] also extended the hydrodynamic penetration model to include non-uniform jet velocity distribution and stand-off distance. This model started from an arbitrarily selected initial time and required the initial jet length at this moment to be given, which makes the model difficult in practical use.

The concept of virtual origin was first proposed by Allison and Bryan [4] and then developed by Allison and Vitali [5] for the penetration of continuous and particulated jets with the consideration of velocity gradient and the stand-off distance between the virtual origin and target surface. This model has been widely accepted, which can be used to predict the depth of penetration before and after jet breakup [2, 6].

The virtual origin model keeps the basic equations in hydrodynamic model, i.e. Eqs.(1) and (3) where the strengths and the compressibility of the jet and target materials were neglected. Eq.(2) was abandoned because the concept of jet length cannot be applied when it is lengthened as it travels forward from the shaped charge. In addition to these assumptions, following conditions for the existence of a virtual origin need to be satisfied.

Existence of a virtual origin: All jet elements are formed simultaneously at a virtual origin located a distance Z_0 in front of the target surface. Each jet element is emitted from the virtual origin at its own velocity that remains constant during its travelling between virtual origin and target. The existence of a unique virtual origin location of the entire jet requires that the spatial distribution of jet velocity is linear.

In the virtual original model and its applications, the density of the jet element is treated as a constant, i.e. the density of each element remains constant during its travelling and the spatial distribution of the jet density is uniform. However, it has been observed that there is a density deficit based on flash x-ray measurements and the soft recovery of jet fragments [7-8]. Variable density distribution was also observed in the jets formed from powdered metal liners [9-11]. Therefore, it is necessary to extend the virtual origin model to the jet with non-uniform density distribution.

This paper keeps the assumption that the density of each jet element remains constant during its travelling, but considers the non-uniform jet density distribution to study its effect on the penetration depth. The non-uniform jet density distributions along its axial distance are estimated numerically using the Autodyn jet formation algorithm for the three liners made from electrolytic OFHC copper, zirconium and copper-tungsten un-sintered powder. An analytical approach is introduced to account for the penetration decrease due to the non-uniform density distribution along its axis. The proposed model is validated by experiments and numerical simulations using Autodyn hydro-code.

A modified virtual origin model with non-uniform distribution of jet density is proposed in Section 2. Section 3 describes the liner manufactures and the experimental set-up configurations. Section 4 introduces the numerical models used to simulate the shaped charge jets and penetrations. Results are presented in Section 5 with further analysis, which is followed by conclusions in Section 6.

PENETRATION ANALYTICAL MODEL

In this paper, we will focus on the jet penetration before or without jet breakup. Figure 1 is a schematic drawing that defines the penetration parameters of a shaped charge jet penetrating into an incompressible target. Z_o is the standoff distance from the virtual origin point to the target surface, t is the penetration time, P(t) is the penetration depth at time (t) and V_j is the impinging velocity of the jet onto the target (observed at the jet/target interface), which equals to the velocity of the jet element that impacts the target at the same moment of time t.

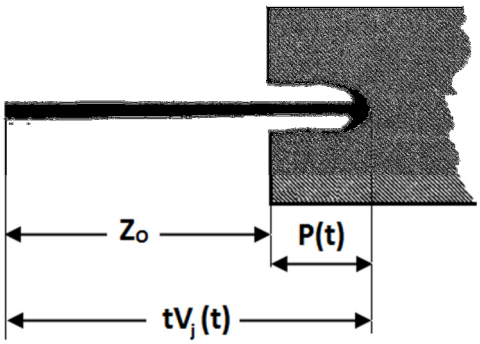

Fig. 1. The hydrodynamic jet penetration [5].

Therefore, the depth of penetration P(t) at a given time t is determined by:

$$P(t) = tV_j(t) - Z_o \quad . \tag{5}$$

The depth of penetration increase monotonically with time, which requires the satisfaction of following condition:

$$\frac{dP}{dt} \geq 0 \text{ for } tV_j(t) \geq Z_o \; . \tag{6}$$

This condition was not checked in previous publications.

When hydrodynamic Bernoulli equation [Eq.(1)] is applied,

$$\mathrm{U} = \frac{\mathrm{V_j}}{\gamma+1} \tag{7}$$

where $\gamma = \sqrt{\rho_T/\rho_j}$.

Following equation can be obtained from Eqs.(3,5,7),

$$V_j(t) + t\frac{dV_j(\mathrm{t})}{dt} = \frac{\mathrm{V_j(t)}}{\gamma+1} \; . \tag{8}$$

When the jet density is a constant, the solution of Eq.(8) predicts the jet velocity $V_j(t)$ as:

$$V_j(t) = V_0 \left(\frac{t_o}{t}\right)^{\frac{\gamma}{\gamma+1}} \quad (9)$$

where V_0 is the jet tip velocity and t_o is the time when the jet tip reaches the target surface (i.e. $t_0 V_0 = Z_0$).

From Eqn.(9),

$$t = t_o \left(\frac{V_0}{V_j(\mathrm{t})}\right)^{\frac{\gamma+1}{\gamma}} , \quad (10)$$

and therefore, the depth of penetration at time t can be obtained from Eq.(5) when $V_j(t)$ and t in Eq.(5) are substituted by Eqs.(9,10)

$$P(t) = Z_0 \left[\left(\frac{V_0}{V_j}\right)^{\frac{1}{\gamma}} - 1\right] = Z_0 \left[\left(\frac{t}{t_0}\right)^{\frac{1}{\gamma+1}} - 1\right] . \quad (11)$$

The maximum penetration is achieved at time t_c when the cut-off jet element (i.e. the last jet element that has hydrodynamic penetration capability) hits the target at the cut-off velocity (V_c). Therefore, the maximum depth of penetration is

$$P = Z_0 \left[\left(\frac{V_0}{V_c}\right)^{\frac{1}{\gamma}} - 1\right] . \quad (12)$$

In the proposed model, it is assumed that the density of each jet element will be a constant during its travel between virtual origin and target. However, since different jet elements have different jet formation processes, their density are different. Therefore, the spatial distribution of the jet density is non-uniform. At the jet-target interface, the observed jet density should be a function of time, i.e. $\rho_j = \rho_j(t)$. Let's ρ_{j0} represent the original density of the liner material and density of target ρ_T is a constant, then $\gamma_0 = \sqrt{\rho_T/\rho_{j0}}$ and $\gamma(t) = \sqrt{\rho_T/\rho_j(t)}$. Thus, $\frac{\gamma(t)}{\gamma_0} = \sqrt{\frac{\rho_{j0}}{\rho_j(t)}}$.

Based on jet formation analysis presented later, it is found that the normalised jet density is directly related to the normalised jet velocity in a linear relationship, as shown in Fig.2. According to Fig.2, the density deficit at the jet tip is larger than that at the rear jet. The maximum density deficits in the simulated examples are around 15.8% reduction for cooper and zirconium liners and 21.7% reduction for copper-tungsten liner, respectively. These values agree with the experimental observations [7]. Details of the numerical simulation will be presented in Sections 4.2 and 5.2.

The linear relationship between $\frac{\gamma(t)}{\gamma_o}$ and $\frac{V_j(t)}{V_0}$ can be described by

$$\frac{\gamma(t)}{\gamma_o} = a\frac{V_j(t)}{V_0} + b \quad (13)$$

where a and b are constants to be determined from data fitting of numerical results and analytical consideration, which will be given at the end of this section.

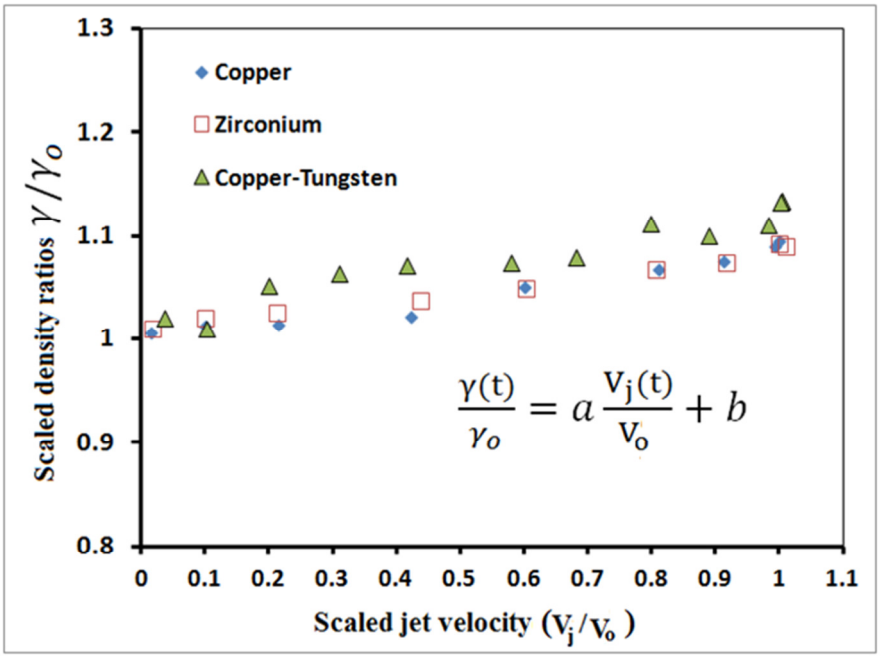

Fig. 2. The relationship between the scaled density ratio and the scaled jet velocity.

Equation (8) can be rearranged as $\frac{-dV_j}{V_j(\tau)} - \frac{dV_j}{\gamma(\tau)V_j(\tau)} = \frac{d\tau}{\tau}$, which can be integrated when Eq.(13) is used, i.e. $\int_{V_0}^{V_j(t)} \frac{-dV_j}{V_j(\tau)} - \frac{1}{\gamma_o}\int_{V_0}^{V_j(t)} \frac{dV_j}{V_j(\tau)\left(\frac{a}{V_0}V_j(\tau)+b\right)} = \int_{t_o}^{t}\frac{d\tau}{\tau}$, or

$$t = t_o\left(\frac{V_0}{V_j(t)}\right)^{1+\frac{1}{b\gamma_o}}\left[\frac{\left(\frac{a}{V_0}V_j(t)+b\right)}{\left(\frac{a}{V_0}V_0+b\right)}\right]^{\frac{1}{b\gamma_o}} \quad . \tag{14}$$

This equation is reduced to Eq.(10) when $\frac{\gamma(t)}{\gamma_o} = 1$ or a=0 and b=1 in Eq.(13).

When $t=t_c$, $V_j(t)=V_c$, the maximum penetration is achieved by the last penetrating element at a cut-off velocity V_c. t_c can be determined by Eq.(14), i.e.

$$t_c = t_o\left(\frac{V_0}{V_c}\right)^{1+\frac{1}{b\gamma_o}}\left[\frac{\gamma_C}{\gamma_t}\right]^{\frac{1}{b\gamma_o}} \tag{15}$$

where $\gamma_c = \sqrt{\rho_T/\rho_{jc}} = \gamma_0\left(a\frac{V_c}{V_0}+b\right)$ and $\gamma_t = \sqrt{\rho_T/\rho_{jt}} = \gamma_0(a+b)$ according to Eq.(13), in which ρ_{jc} and ρ_{jt} are the densities of last penetrating element and tip element of the jet, respectively.

From Eq.(14), the impact velocity of the jet is determined by an algebraic equation of

$$b\left(\frac{V_0}{V_j}\right)^{b\gamma_0+1} + a\left(\frac{V_0}{V_j}\right)^{b\gamma_0} = (a+b)\left(\frac{t}{t_0}\right)^{b\gamma_0} \quad . \tag{16}$$

Eqn. (16) reduces to Eq.(9) for constant jet density when a=0 and b=1.

The penetration depth at time t is determined by Eq.(5) when t is substituted from Eq.(14)

$$P(t) = Z_0 \left[\left(\frac{V_0}{V_j}\right)^{\frac{1}{b\gamma_o}} \left(\frac{a\frac{V_j}{V_o}+b}{a+b}\right)^{\frac{1}{b\gamma_0}} - 1 \right], \quad (17)$$

which can be reduced to Eq.(11) for constant jet density when a=0 and b=1. The solution of Eq.(16) is needed to give an explicit expression of P(t) in Eq.(17).

The maximum depth of penetration is given by:

$$P = Z_0 \left[\left(\frac{V_0}{V_c}\right)^{\frac{1}{b\gamma_o}} \left(\frac{a\frac{V_c}{V_o}+b}{a+b}\right)^{\frac{1}{b\gamma_0}} - 1 \right] = Z_o \left[\left(\frac{V_0}{V_c}\right)^{\frac{1}{b\gamma_o}} \left(\frac{\gamma_c}{\gamma_t}\right)^{\frac{1}{b\gamma_o}} - 1 \right], \quad (18)$$

when $V_j=V_c$ and $t=t_c$. Eq.(18) is reduced to Eq.(12) for constant jet density when a=0 and b=1 or when $\gamma_c=\gamma_t=\gamma_o$ and b=1.

The values of 'a' in Eq.(13) were determined from the curve fitting of γ-V_j relationship along the jet length in Fig.2, which are shown in Table 1.

Table 1. The values of parameters a and b in Eq.(13).

Curve fitting		a [Eq.(19)]
a	b	
0.077	1.0082	0.080
0.089	0.9983	0.086
0.107	1.0179	0.096

It was further found that parameter a is correlated with the density of the liner material (ρ_{j0}), the standoff distance (Z_o), the total mass of the jet (m_{jet}) from the standard jetting analysis and the radius of the jet (r) from jet formation simulation or flash X-ray experiment. A non-dimensional formula can be recommended for the calculation of parameter a, i.e.

$$a = \frac{m_{jet}}{\rho_{j0}\ \pi\, r^2 Z_o}\ . \quad (19)$$

The values of 'a' using Eq.(19) are also listed in Table 1 for three liner materials. It can be seen that values of a predicted by Eq.(19) are very close to the corresponding values determined by curve-fitting method. According to Table 1, the values of 'b' can be approximated to unity for the three liner materials.

LINER MATERIALS AND PENETRATION EXPERIMENTS

The three liners that have been used in this study were the copper, the zirconium and the un-sintered copper-tungsten powder. The liner has a small base diameter of 33mm, a cone apex angle of 46 degree and a varied liner wall thickness as illustrated in Figure 3.

The copper liner was OFEC (Oxygen Free Electrolytic Copper) of grade C10100 with purity of 4N (99.99%). It was manufactured using the deep drawing technique with an intermediate annealing of 1000^{o}C (two minutes) to decrease the strain hardening and maintain the material ductility [12].

The zirconium liner was manufactured from a solid pure Zirconium cylinder 4N (99.9951) having a density of 6623kg/m^3 using high accuracy CNC machine in order to guarantee a high precision manufacturing (i.e. the precision of 5μm). The Zirconium rod was annealed to 900^{o}C for one hour before machining in order to obtain a relative small average grain size, hence to increase its ductility, which in turn will increase its breakup time and improve the liner performance [13]. The type and the percentage of the impurities present in the Zirconium material are listed in Table 2.

Table 2. The elemental percentage of impurities presented in the Zirconium material.

Element	Impurities amount (%)
Fe	0.0050
Cr	0.0009
C	0.0010
N	0.0080

Powder metallurgy (PM) technique has been used to manufacture OWP liners. It has good penetration capability especially at short stand-off distances [14-17]. The composition of the powder mixture ingredients is listed in Table 3. Small average grain size with irregular particles shapes are chosen for the liner powders. The powders are mixed together with the designated mass ratio until the homogeneous mixture blend is obtained, after which they are pressed using the punch, the die and the ejector, shown in Figure 4. The applied pressure was 100MPa using hydraulic press at a low rate (i.e. 1MPa per second) to avoid trapping air voids inside the liner material. The product is a brittle material in the pre-sintering state and is called 'the green', which is tested in this state without sintering. All three tested liners are show in Figure 5.

Table 3. The mass percentage of the powder liner composition.

Material	Copper	Tungsten	Tin	Graphite
Mass ratio %	43	45	11	1
Average grain size	3	0.6:1	< 45	< 20
Function	Binder	Main powder	Binder	Lubricant

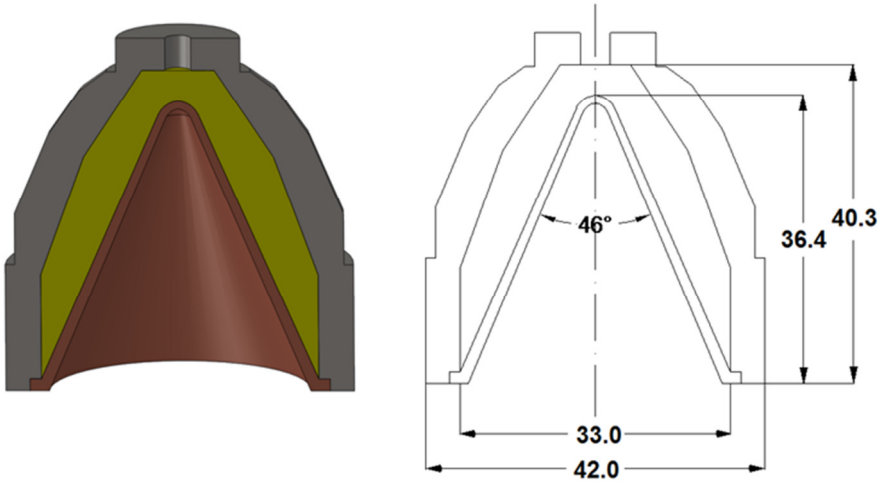

Fig. 3. A sketch of the designed shaped charge well perforator.

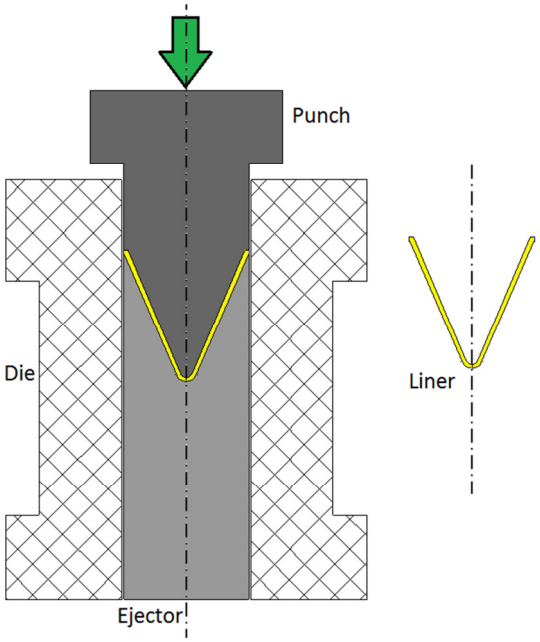

Fig. 4. A sketch of the punch, the die, the ejector and the produced powder liner.

The powder liner density is not uniform over the entire liner height because the force distribution is not homogeneous due to the conical liner profile. Therefore, small parts of the same powder liner specimen were cut off and used to measure their densities using the gas pycnometer [18]. The measured densities for the testing specimens as a function of the scaled distance from the cone apex to the liner height are shown in Figure 6, which is taken into account in the description of liner physical properties in Autodyn hydro-code simulations.

The charge casings are steel with an average wall thickness of 4.5mm. The main explosive charges for the three charges are PE4 with a total average mass of 24.5g and a standard deviation of 0.8g. The PE4 explosive is a powerful RDX-based explosive (i.e. 88% RDX in mass, 12% plasticizer and other additives) having a

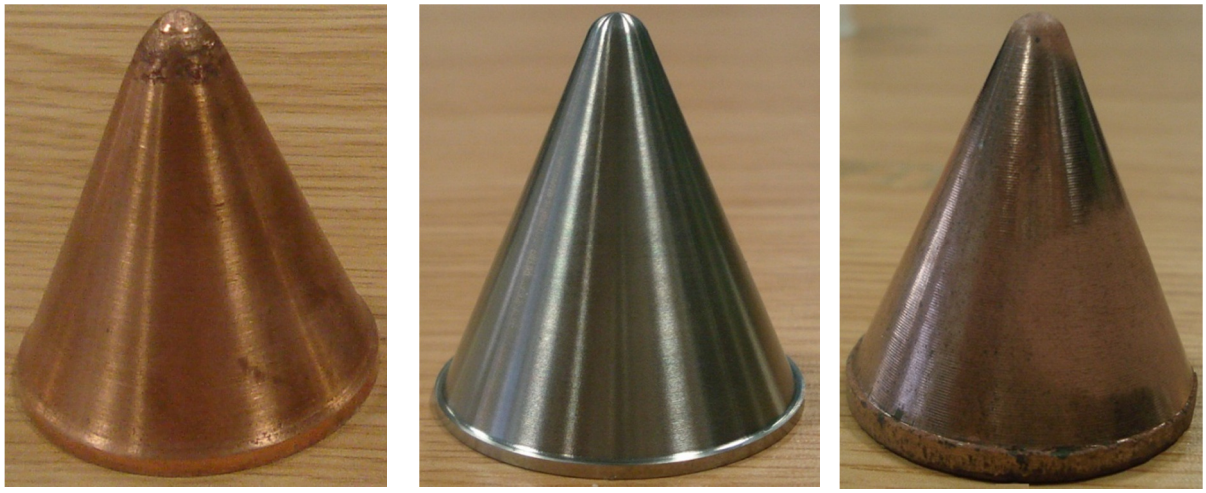

Fig. 5. The studies three liners.

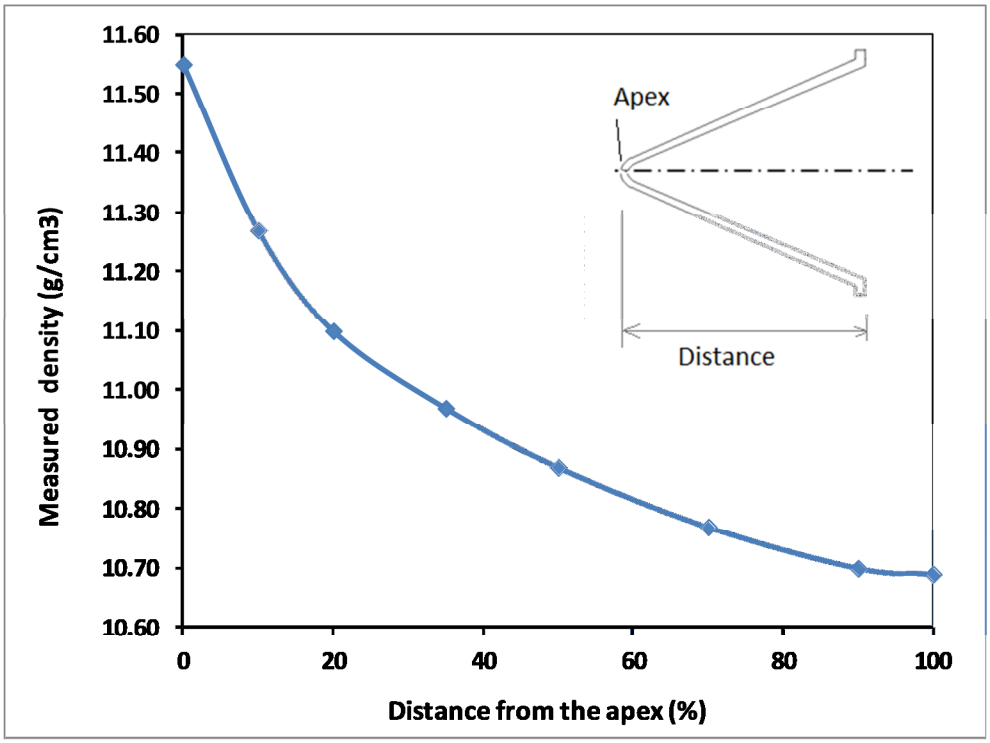

Fig. 6. The measured densities of the liner elements at different distances from the cone apex point.

detonation velocity of 8027m/s at 1.59g/cm^3 density [19] and 8200m/s at 1.6g/cm^3 density [20]. The explosive charge was filled into the steel casing first. Then, the liner was pressed slowly against the steel casings containing explosives to avoid holding air gaps inside the explosive. The charges were then attached to the upper steel layer of the test configuration as shown in Figure 7.

The Concrete cylinders with the designated strength value were casted from the same mixture and allowed to cure according to the test evaluation of the well perforator [21]. These targets were tested according to the standard OWP testing configuration and requirements in the Section-II of API-RP43 [22]. The measured average strength of the standard concrete cubes was 40.02 MPa with a standard deviation of 0.92 MPa, measured at 28 days after their casting [23].

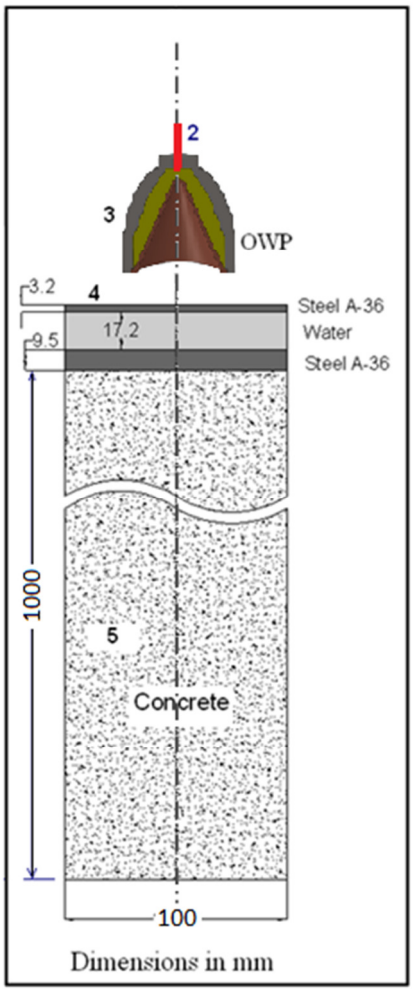

Fig. 7. Dimensions of the test setup and the experimental test configuration (2: Boaster; 3: OWP; 4: Front steel disc; 5: Concrete; 6: power supply cable).

In a separated test without target, the particulated copper jet fragments were recovered using sand. The densities of two jet fragments were measured using helium gas pycnometer, which has an accuracy of 10^{-4} g/cm^3. The measured densities of the two jet fragments were 7.4120 and 8.2300 g/cm^3 at the tip and the rear, respectively. In comparison with the original density of copper liner material (8.930 g/cm^3), they represent 17.0% and 7.8% density deficits, respectively. The density deficit at the tip of jet (17.0%) is very close to the maximum density deficit predicted in Fig.2 (15.8%). This again gives evidence to support the existence of density deficit in the formed jet of a shaped charge, which was first observed based on X-ray measurements [7-8].

NUMERICAL MODELS

Hydrocode Algorithms of the Jetting Analysis, the Jet Formation Model and the Jet Penetration Model

Autodyn hydro-code is used in this paper through three algorithms, Shell jetting analysis, Euler jet formation model and Lagrange-Lagrange jet penetration model [24].

The jetting analysis is based on the analytical unsteady PER model [25]. PER model is solved numerically using finite difference technique to calculate the jet and slug velocities, jet and slug masses and the collapse and deflection angles of the jet elements. The shaped charge jetting analysis was validated by comparing the jetting analysis results of the 90mm shaped charge with real experimental results [26]. The jet formation modelling is performed using Euler method based on continuum mechanics to obtain the jet profiles at different time stages. In this scheme, the explosive, the charge casing and the liner materials are filled into the global Euler multi-material part [24]. This processor is suitable in the early jet formation stages where large distortions are caused by extremely high strain-rate in the order of $10^7 s^{-1}$. The evolved jet is allowed to move on the Euler grids up to the moment when the first jet element starts to impact the target. At this moment, the formed jet is remapped as a Lagrangian mass having non-uniform velocity distribution. Then, it is exported to the Lagrange-Lagrange jet penetration model for penetrate analysis where both jet and target consisting of steel, water and concrete are described in Lagrange method.

Mesh Sensitivity for the Jet Formation Model

In order to study the mesh sensitivity on the jet characteristics, five different mesh densities were proposed for the jet formation modelling. The jet formation was used to identify the density and velocity of the jet elements as they pass the gauge point shown in Figure 8. The fixed gauge point is located 100mm from the liner base (i.e. 3 time calibre). The uniform square meshes of 0.17, 0.2, 0.25, 0.33 and 0.50mm of the Euler grids were used for mesh sensitivity analysis in the jet formation model.

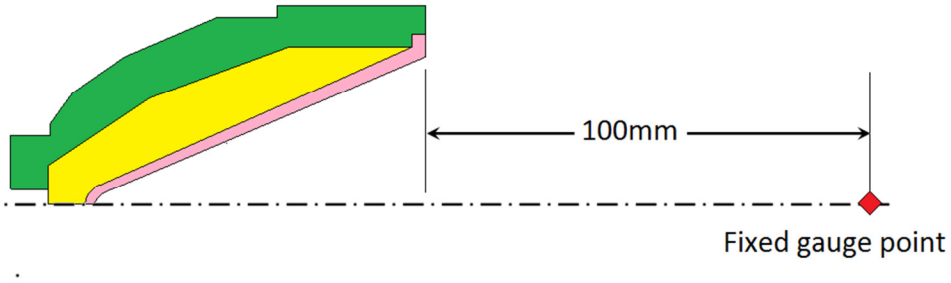

Fig. 8. Location of the fixed gauge point used to predict the density and the velocity histories for the mesh sensitivity study.

Figure 9 shows the recorded density history at the fixed gauge point using five mesh sizes. The density histories for the five mesh sizes are detected between 14 and 16 μs. It shows that finer mesh sizes give higher densities at the beginning. But the density corresponding to each mesh size convergences to the copper solid material

density as the jet tail passes through the gauge point. This means that the density of the jet material increases gradually from the tip to its tail due to the existence of velocity gradient. The maximum relative difference of density for the finest and coarsest meshes is about 7%.

The velocities of jet elements passing the gauge point are obtained by the same way used for the calculation of density. The velocity histories for different mesh sizes are depicted in Figure 10. It can be observed that the five meshes predict nearly the same shape of the velocity history. The relative difference of the peak velocity between coarsest and finest meshes is 14.8% while the relative difference of the peak velocity between the finest and second finest meshes is reduced to 2.9%, which indicates the convergence with the decrease of mesh size. These evidences ensure that a mesh size of 0.17mm is sufficient while practically affordable, which will be used globally for the calculations of jet velocity and density.

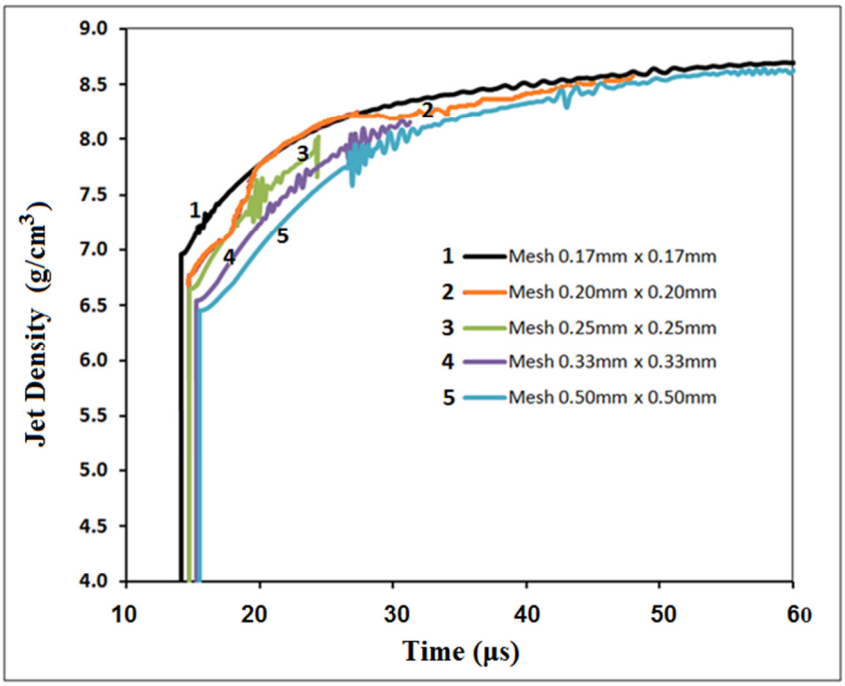

Fig. 9. The recorded density-time histories for the fixed gauge point using five different mesh sizes.

Mesh Sensitivity for the Jet Penetration into Target

In order to find the influence of mesh size on the penetration depth into target, five different mesh sizes were used for the laminated target consisting of steel, water and concrete (their dimensions have been shown in Fig.7) while the copper jet mesh density remains unchanged for all five models. The different uniform square mesh sizes of 0.5, 1, 2, 3 and 4mm were used for the laminated target. The penetration depths into the target using different mesh sizes are shown in Figure 11. It is evident that the penetration depth is convergent with the reduction of mesh size. The relative difference of the penetration depth for 0.5 and 1.0mm meshes is only 0.3%. However, the simulation time for 0.5mm mesh is doubled (170 hours). Therefore, the mesh size of 1mm×1mm is used globally for the penetration analyses of three liners.

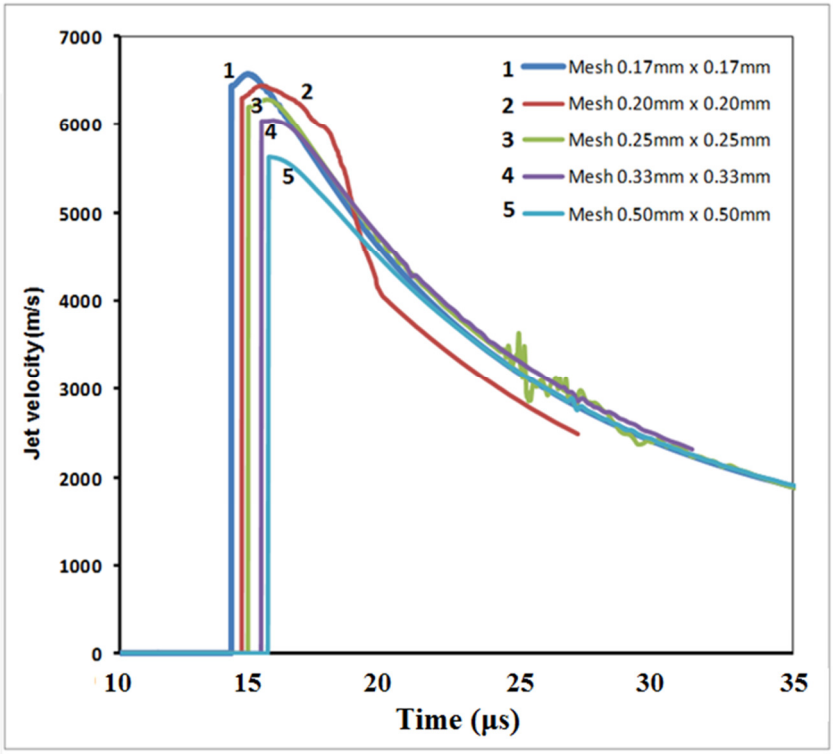

Fig. 10. The recorded velocity-time histories for the jet material particles moving through the gauge point.

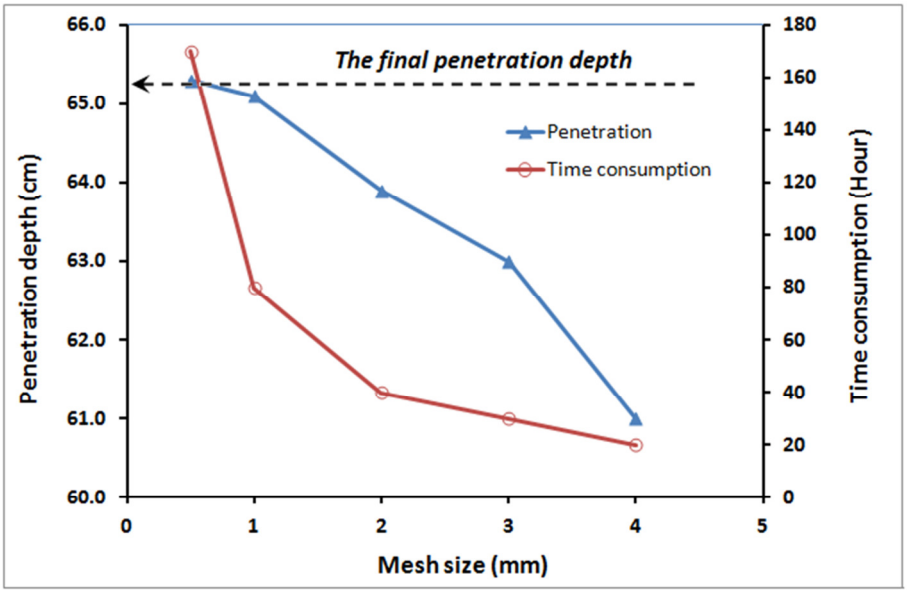

Fig. 11. The penetration depths into laminated target using different mesh sizes and the relevant time consumption.

RESULTS

The Jetting Analysis Results

The outputs of the jetting analysis for the shaped charge perforators with three different liners are summarized in Table 4. The kinetic energies of the three produced jets nearly have the same value of 36 kJ because they have the same liner shape and the same amount of explosive. However, the Zirconium liner with the lowest density and mass has the highest jet tip velocity of 6075m/s but with the lowest jet mass of 3.1g.

Table 4. The different liners and their jet characteristics.

Liner material	Copper	Zirconium	Powder
C_o (m/s)	3757	3940	3849
Liner mass (g)	32.6	25.1	40.2
Jet mass (g)	4.0	3.1	4.5
Jet % from the liner	12.31	12.53	11.18
Jet K.E. (kJ)	36.0	37.2	35.7
Jet tip velocity (m/s)	5476	6075	5320
Cut-off velocity (m/s)	1610	1720	1747
Time (t_o at Z_o) (μs)	18.50	16.52	19.30
Initial Z_o (cm)	10.7	11.5	12.2

Jet Density Distribution

The density of the jet along its length was calculated from the jet formation model for three liners where Mie-Gruneisen EOS based on the shock Hugoniot was used. The density of the collapsed liner material is directly related to the liner compressibility and the pressure generated from the explosive load. Distributions of density, compressibility and velocity over the entire jet length are depicted in Figure 12 for the copper jet. This figure shows that jet density decrease from slug to tip along the jet. Besides, the density contours also shows a radial density distribution on the circular cross-section of the jet (i.e. the density at tip premises is 0.6% larger than that at its centreline). Figure 13 shows the velocity and the density histories of the copper jet recorded at the fixed gauge point. The distributions of jet density and velocity along the jet axis for the copper liner at a given time are shown in Figure 14. Both figures 13 and 14 demonstrate the increase of density deficit with the corresponding jet velocity.

The projected effective jet lengths for the three shaped charge perforators with different liners were calculated by the back projection of the relation between time and effective jet length from the moment when the jet reaches the first steel layer. An example of the relation between time and effective jet length established by the data obtained from Autodyn jetting analysis is shown in Figure 15. However, this value cannot be used directly with Eq.(18) because the effective jet length has to be modified with considering the thicknesses of the laminated steel and water layers.

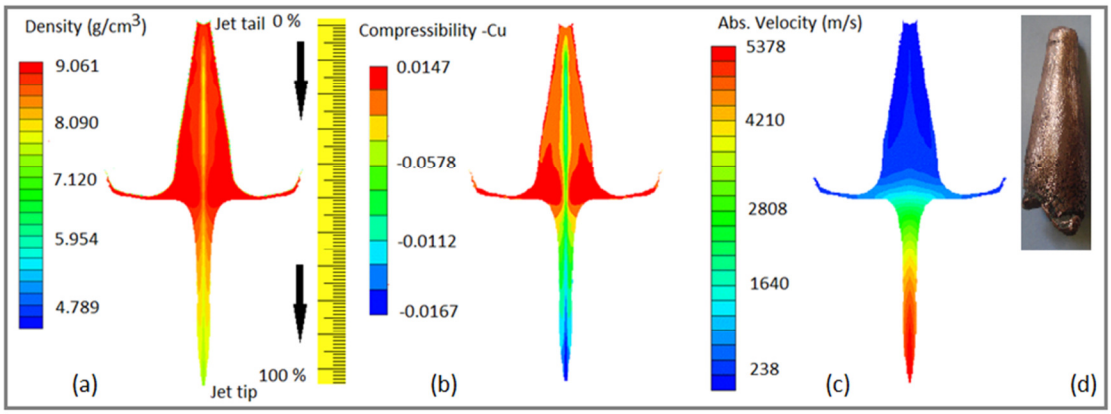

Fig. 12. Density (a), compressibility (b) and velocity (c) of the copper jet just before the jet tip impacts on the target; (d) a picture of the recovered copper slug.

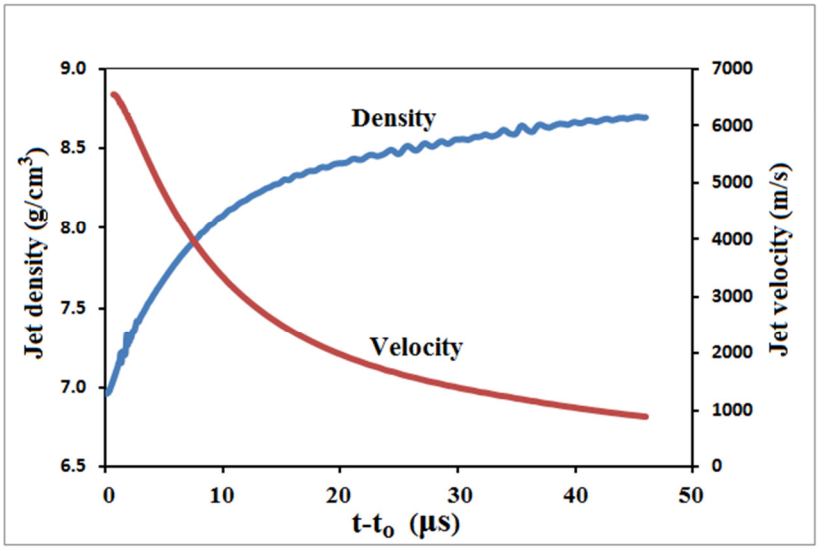

Fig. 13. Jet velocity and density histories recorded at a fixed gauge point.

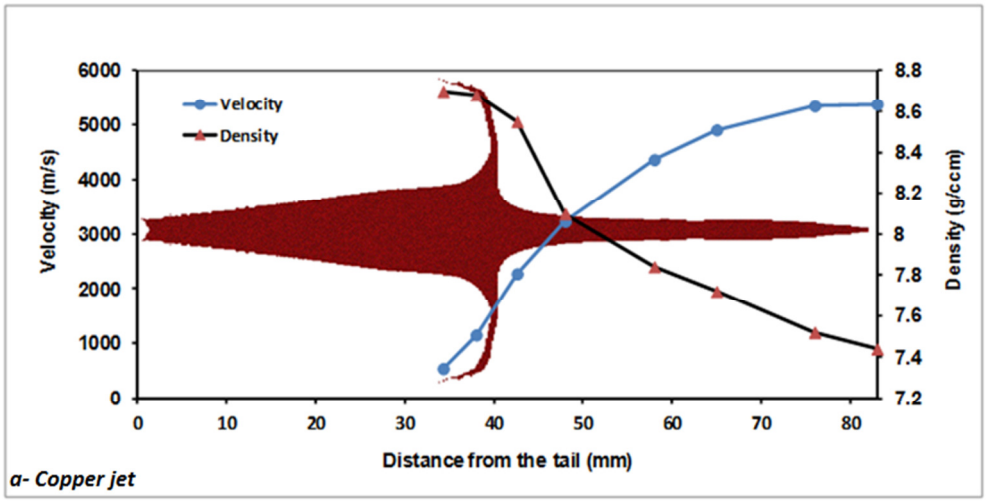

Fig. 14. Jet density and velocity distributions along the jet axis for copper liner.

The Penetration Depth Calculations

The projected effective jet lengths for the three shaped charge perforators with different liners were calculated by the back projection of the relation between time and effective jet length from the moment when the jet reaches the first steel layer. An example of the relation between time and effective jet length established by the data obtained from Autodyn jetting analysis is shown in Figure 15. However, this value cannot be used directly with Eqn.(18) because the effective jet length has to be modified with considering the thicknesses of the laminated steel and water layers.

The jet tip velocity correction based on the uniform density distribution, i.e. Eq.(12), for the exit jet tip velocity perforating a finite thickness target [2] has the form of:

$$V_{jex} = V_{jin}\left(\frac{Z_i}{Z_i+T_i}\right)^{\gamma_i} \tag{20}$$

where V_{jex} and V_{jin} are the exit and the input jet tip velocities, respectively; Z_i is the effective jet length at the front of the target surface, T_i is the target thickness and i refers to the number of the target layer to be perforated.

However, Eqn. (20) is not suitable for the penetration formula, Eqn. (18), where non-uniform density effect is considered. Thus Eqn. (20) was modified based on Eqn. (18) to determine the exit jet velocity with considering the density reduction effect,

$$V_{jex} = \frac{bV_{jin}}{(a+b)\left(\frac{Z_i+T_i}{Z_i}\right)^{b\gamma_i}-a} \quad . \tag{21}$$

Equation (21) together with Eqn. (18) can be used to predict the penetration depth of a shaped charge jet into a multi-layered target when the non-uniform density distribution of the jet is considered. The values of the exit jet tip velocity and the relevant effective jet length for the test layers are illustrated in Table 5 while Table 6 presents the penetration depth calculated using various methods including the modified virtual origin model [Eqn. (18)] in Section 2, and the penetration reduction due to the density gradient (deficit).

The calculated penetration depths and the reduction percentages in penetration due to the density gradient along the jet length indicate that the reduction term has considerable influence on the predicted penetration depth of a shaped charge jet. Data in Table 6 are presented in Fig.16. It clearly shows that the modified virtual origin model largely improve the predictions of penetration depth by virtual origin model for all three liners.

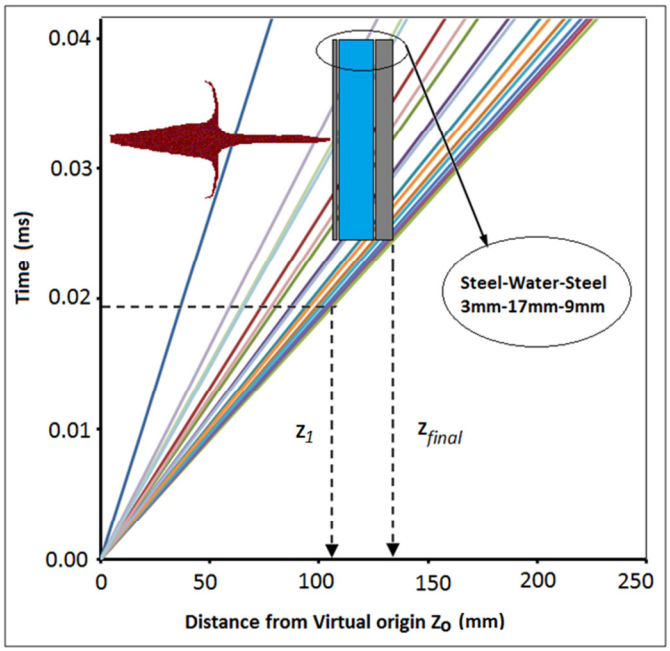

Fig. 15. The fan plot of the copper jet showing the original and the modified effective jet length due to the presence of the laminated test layers.

Table 5. The effective jet length and the jet exit velocities of the three test layers.

Property	Zirconium	Copper	Powder
V_{tip} (m/s)	6075	5476	5320
V_{cutoff} (m/s)	1620	1610	1747
Z_o (cm)	11.5	10.7	12.2
Solid jet density ; ρ_j (g/cm^3)	6.51	8.93	11
Target density ; ρ_T (g/cm^3)	2.75	2.75	2.75
$\gamma=(\rho_t/\rho_j)^{\wedge}0.5$	0.65	0.55	0.50
Vp_1 (m/s); Eq.(21)	5891.8	5324.2	5198.9
Vp_2 (m/s); Eq.(21)	5564.5	5053.7	4979.3
Vp_3 (m/s); Eq.(21)	5153.9	4714.4	4698.1
Vp_3 (m/s); Eq.(20)	5219.5	4769.7	4762.1
Z_{final} (cm)	14.4	13.6	15.1

Table 6. Comparison among experimental result, numerical simulation and the virtual origin model predictions for the penetration of jets with three different liners.

	V_j (m/s) Eq.(20)	V_c (m/s)	a Value	Penetration depth (cm)				Reduction	
				VO Eq.(12)	Modified VO Eq.(18)	Exp.	Sim.	(cm)	(%)
Zirconium	5153.9	1620	0.077	72.73	63.57	68.0	59.0	9.20	12.5
Copper	4714.4	1610	0.089	82.67	72.04	64.0	65.0	10.63	12.8
Powder	4698.1	1747	0.049	97.10	78.18	80.0	75.0	18.91	19.4

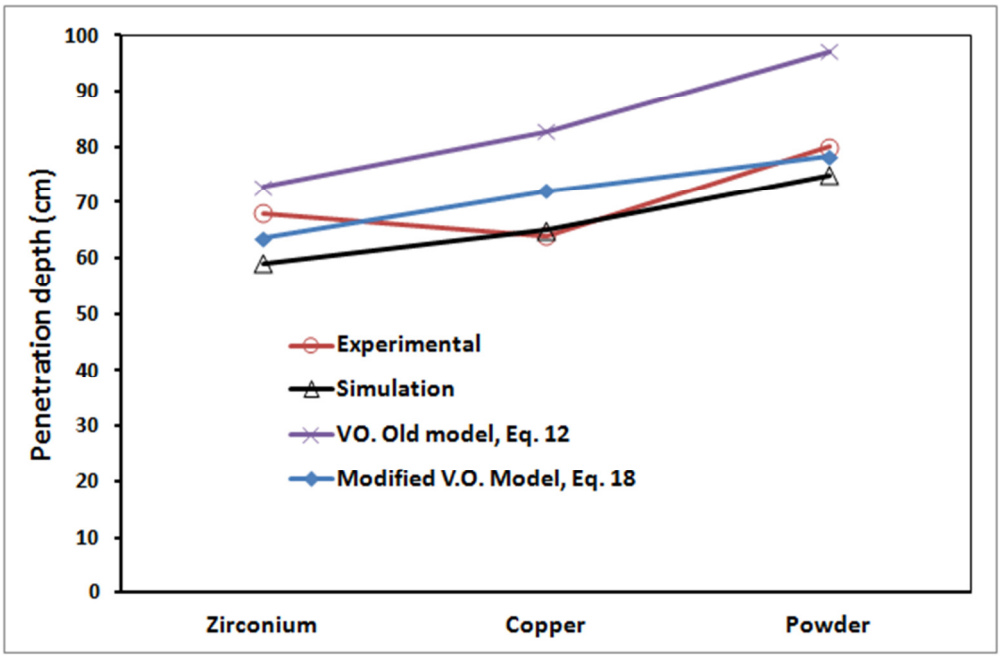

Fig. 16. Comparison among experimental result, numerical simulation and the virtual origin model predictions for the penetration of jets with three different liners.

CONCLUSIONS

The density deficit of a shaped charge jet is developed during the jet formation, which has been shown experimentally and numerically in this paper. This leads to the non-uniform distribution of the jet density and the original virtual origin penetration model is incapable of dealing with penetration of jet with uniform density distribution. A correlation between jet density deficit and jet velocity is proposed in this paper, based on which an analytical solution of the modified virtual origin model is obtained. The validity of the modified virtual origin model is demonstrated by its largely improved predictions in comparison with experimental and numerical results.

ACKNOWLEDGEMENT

The authors thank Event Horizon Ltd for the filling and testing of the shaped charge perforators, Dr Steve Burley for his technical support and the University of Nottingham for the use of the helium gas Pycnometer facility.

REFERENCES

[1] G. Birkhoff, D. P. Macdougall, E. M. Pugh, and G. Taylor, “Explosives with lined cavities”, Journal of Applied Physics, , 19, p. 563(1948).

[2] W. P. Walters, W. J. Flis, P. C. Chou, “A survey of shaped-charge jet penetration models”, International Journal of Impact Engineering, 7, 8, p. 307(1988).

[3] G. R. Abrahamson and J. N. Goodier, “Penetration by Shaped Charge Jets of Nonuniform Velocity", Journal of Applied Physics, p. 195(1963).
[4] B. G. M. Allison F.E., “Cratering by a train of hypervelocity fragments”, Proceedings of the 2nd Hypervelocity Impact Effects Symposium. , p. 1. (1957).
[5] F. E. Allison and R. Vitali, “A new method of computing penetration variables for shaped charge jet”, Ballistic Research Laboratory Report No. 1184, (1963).
[6] J. Simon, R. Dipersio, A. B. Merendino, “Penetration of shaped-charge jets into metallic targets”, Ballistic Research Laboratory Memorandum Report No. 1296, (1965).
[7] L. Zernow, “The density deficit in stretching shaped charge jets”, International Journal of Impact Engineering, 20, p. 849 (1997).
[8] F. Jamet, “Measurements of densities in shaped charge jets and detonation waves”, American Society for Non-Destructive Testing, (1976).
[9] K. D. Werneyer, F. J. Mostert, “Analytical model predicting the penetration behaviour of a jet with a time-varying density profile”, 21st International symposium on Ballistics, South Africa, p. 390 (2004).
[10] M. F. Maritz, K.D. Werneyer and F. J. Mostert, “An analytical penetration model for jets with varying mass density profiles”, 22nd International symposium on Ballistics, Canada. p. 622 (2005).
[11] B. Grove and I. Walton, “Shaped Charge Jet Velocity and Density Profiles”, 23rd International Symposium on Ballistics, Spain (2007).
[12] M. Held, “Liners for shaped charges”, Journal of Battlefield Technology, 4, (2001).
[13] R. H. Nielsen, “Zirconium and Zirconium Compounds”, ULLMANN’S Encyclopedia of Industrial Chemistry, vol. 39, p. 753 (2012).
[14] B. Zygmunt and Z. Wilk, “Formation of jets by shaped charges with metal powder liners”, Propellants, Explosives, Pyrotechnics, 33, p. 482 (2008).
[15] D. J. Leidel and J. P. Lawson, “High performance powder metal mixtures for shaped charge liners”, USA Patent No. US 7,547,345 B2, (2009).
[16] L. Yingbin and S. Zhaowu, “Numerical simulation on formation and penetration target of powder metal shaped charge jet”, International Conference on Computer Application and System Modelling (ICCASM), 9, p. 518 (2010).
[17] W. Walters, P. Peregino and R. Summers, “A Study of jets from un-sintered powder metal lined non-precision small calibre shaped charge”, Army Research Lab. No. MD 21005-5066, (2001).
[18] Micromeritics, http://www.micromeritics.com/product-showcase/accupyc-ii-1340.aspx. (2012).
[19] M. C. Chick. and L. A. Learmonth, “Determination of shock initiation and detonation characteristics of PE4 in proof test geometries”, Report No. MRL-R-979, (1986).
[20] R. K. Wharton, S. A. Formby and R. Merrifield, “Airblast TNT equivalence for a range of commercial blasting explosives”, Journal of Hazardous Materials, 79, p. 3 (2000).
[21] W. Porter and B. Satterwhite, “Evaluation of Well Perforator Performance”, Journal of Petroleum Technology, 28, p. 1466 (1976).
[22] API, Evaluation of Well Perforators, “Recommended Practice RP 43”, American Petroleum Institute (API). USA, (1991).
[23] ASTM, “Standard Practice for Making and Curing Concrete Test Specimens in the Laboratory”, vol. 04, (2002).

[24] Autodyn Team, Autodyn theory manual, 3rd Revision, Century Dynamics, USA, (1997).
[25] E.M. Pugh, R.J. Eichelberger, and N. Rostoker, "Theory of jet formation by charges with lined conical cavities". Journal of Applied Physics, 23, 5, p. 532. (1952).
[26] Autodyn Team, "Autodyn jetting tutorial", 3rd Revision, Century Dynamics, USA, (1997).
[27] C.M. Tarver, W.C. Tao, and C.G. Lee, "Sideways Plate Push Test for Detonating Solid Explosives", Propellants, Explosives, Pyrotechnics, 21, 5, p. 238 (1996).
[28] B. M. Dobratz, P. C. Crawford, "Explosives Handbook: Properties of Chemical Explosives and Explosive Stimulants", Lawrence Livermore National Laboratory, UCRL, CA (1985).
[29] G. Johnson and W. Cook. "A Constitutive Model and Data for Metals Subjected to Large Strains", High Strain Rates and High Temperatures. Proceedings of the 7th Int. symposium on ballistics. (1983).
[30] W. Herrmann, "Constitutive Equation for the Dynamic Compaction of Ductile Porous Materials", Journal of Applied Physics, 40, 6, p. 2490 (1968).
[31] H. Heider and S. Hiermaier, "Numerical Simulation of the Performance of Tandem Warheads", 19th International Symposium of Ballistics, Interlaken, Switzerland, (2001).
[32] W. Riedel, K. Thoma, S. Hiermaier and E. Schmolinske, "Penetration of Reinforced Concrete by BETA-B-500. Numerical Analysis using a New Macroscopic Concrete Model for Hydrocodes, 9th International Symposium on the Interaction of the Effects of Munitions with Structures, (1999).
[33] Z. Tu and Y. Lu, "Evaluation of typical concrete material models used in hydrocodes for high dynamic response simulations", International Journal of Impact Engineering, 36, p. 132 (2009).
[34] V. S. Berg, D.S. Preece, "Shaped charge induced concrete damage predictions using RHT constitutive modeling", Journal of International Society of Explosives Engineers 2 (2004).
[35] J. Leppänen, "Concrete Structures Subjected to Fragment Impacts", PhD thesis, Chalmers University of Technology, Göteborg, Sweden, (2004).
[36] J. C. Hayhurst, A. C. Richard, I. H. Livingstone and N. J. Francis, "The application of SPH techniques in Autodyn 2-D to ballistic impact problems", 16th International Symposium on Ballistics, San Francisco, USA, (1996).
[37] B. Adel, "Numerical approach in predicting the penetration of limestone target by an ogive-nosed projectile using Autodyn 3-D", 12th International Colloquium on Structural and Geotechnical Engineering (ICSGE), Egypt. (2007).